Geomechanics and Engineering, *Vol. 34, No. 1 (2023) 87-102*
https://doi.org/10.12989/gae.2023.34.1.087

Deformation characteristics and stability analysis of semi-covered deep excavations with existing buildings

Linfeng Wang[1,2,3], Xiaohan Zhou[*1,2,3], Tao Chen[4], Xinrong Liu[**1,2,3], Peng Liu[1,2,3], Shaoming Wu[5], Feng Chen[5] and Bin Xu[1,2,3]

[1]*College of Civil Engineering, Chongqing University, Chongqing 400045, China*
[2]*State Key Laboratory of Coal Mine Disaster Dynamics and Control, Chongqing University, Chongqing 400044, China*
[3] *National Joint Engineering Research Center for Prevention and Control of Environmental Geological Hazards in the TGR Area, Chongqing 400045, China*
[4]*China Railway Major Bridge Reconnaissance & Design Institute Co., Ltd., Wuhan Hubei 430050, China*
[5]*Guangzhou Expressway Co.,Ltd., Guangzhou Guangdong 510000, China*

(*Received June 29, 2021, Revised May 18, 2023, Accepted May 25, 2023*)

Abstract. The cover plate and the building loads often make the semi-covered deep excavations with existing buildings bearing asymmetric load, presenting different deformation characteristics with normal excavations, which is not absolutely clear in current studies. Based on a typical engineering, the building storeys, the basement storeys, the pile length, the existence of the cover plate (CP) and the depth of the diaphragm walls (DW) were selected as variables, and 44 groups of simulation were designed to study the influence of existing buildings and the semi-covered supporting system on the deformation of the excavations. The results showed that the maximum lateral displacement of DW, δ_{hm}, and the depth of δ_{hm}, H_m, are affected seriously by the building storeys and the basement storeys. Asymmetric structures and loading lead to certain lateral displacement of DW at the beginning of excavation, resulting in different relationships between δ_{hm} and excavation depth, H. The maximum surface settlement outside the pit, δ_{vm}, increases significantly and the location, d_m, moves away from the pit with the building storeys increases. δ_{vm} has a quadratic correlation with H due to the existing buildings. CP and building load will affect the style of the lateral displacement curve of DW seriously in different aspects.

Keywords: deep excavation; deformation characteristics; existing buildings; numerical simulation; semi-covered method

1. Introduction

Continuing urban development making available underground space constantly reduced, leading to more and more underground projects facing complex construction environment and strict construction requirements. At the same time, more attentions have been paid to the deformation and destruction of surrounding buildings caused by excavation. Excavation adjacent to the buildings will cause the deformation of the ground and settlement, deflection and even crack of the nearby buildings (Capraru and Adam 2014, Rotisciani *et al.* 2016, Xiang *et al.* 2018, Zhang *et al.* 2018, Zhang *et al.* 2018, Nisha *et al.* 2019, Qian *et al.* 2020, Liu *et al.* 2022a). The influence of deep excavations on surrounding piles is mainly reflected in the change of stress on pile - soil interface, which leads to settlement and lateral displacement of the piles and the surrounding soils simultaneously. Related researches mainly focus on the load transfer mechanism of the piles (Zhen *et al.* 2012, Ng *et al.* 2017, Li *et al.* 2019) and main influencing factors (Korff 2013, Soomro *et al.* 2019).

Bottom-up method is usually used to construct deep excavations with small volume, relatively simple environment and less construction difficulty due to the lower construction cost and the faster construction speed (Khoiri and Ou 2013, Chen *et al.* 2015, Whittle *et al.* 2015, Orazalin *et al.* 2015, Hsiung *et al.* 2016, Lim *et al.* 2016, Houhou *et al.* 2019, Mansouri and Asghari 2019).

Compared with bottom-up method, top-down method can not only provide stronger supporting conditions, but also meet the traffic demand during construction, and is widely used in urban deep excavations (Arboleda-Monsalve and Finno 2015, Jamsawang *et al.* 2017, Jamsawang *et al.* 2019). Most of the metro stations are located in dense urban areas. Considering the deformation of the surrounding buildings and the traffic demand, top-down method is usually adopted (Likitlersuang *et al.* 2013, Hsiung *et al.* 2018, Guo *et al.* 2019). Semi-covered method is a new construction method which was first put forward and applied in the construction of the New Northeast Line of Singapore Rail Transit (Mitchell *et al.* 2000). And it has been used and improved over the last 20 years (Talha 2001, Tian *et al.* 2010, Li *et al.* 2013, Tan *et al.* 2017, Liu *et al.* 2019). It is inherently a bottom-up method and has all the advantages of the bottom-up method, but it can effectively relieve the traffic during the construction due to the cover plate. Besides, the cover plate has stronger stiffness than struts, and is no doubt helpful to control the soil

*Corresponding author, Associate Research Fellow
E-mail: zhouxh2008@126.com
**Corresponding author, Professor
E-mail: liuxrong@126.com

ISSN: 2005-307X (Print), 2092-6219 (Online)

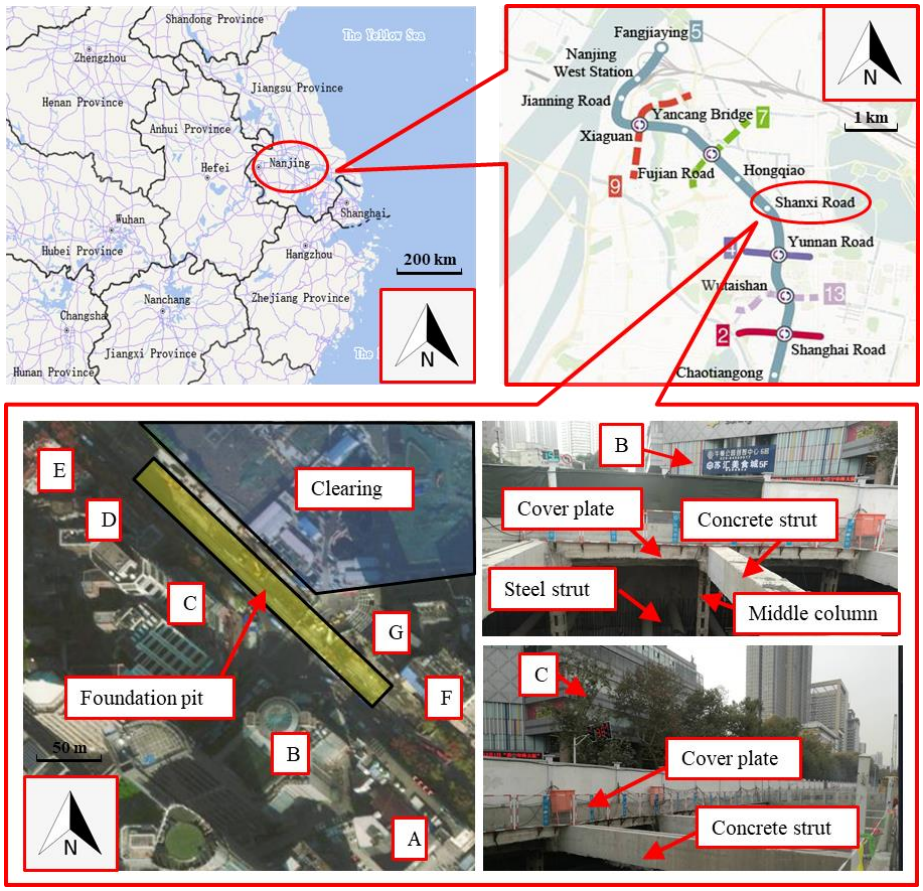

Fig. 1 Location of the foundation pit and the surrounding environment (The map on the top left is obtained from Omap and that on the left bottom is from Baidu Map; A-G are the surrounding buildings)

deformation near the pit.

In existing literatures, Talha (2001), Tian *et al.* (2010) carried out the numerical simulation of semi-covered deep excavations in Kuala Lumpur and Singapore, respectively, which proves the positive role of semi-covered method in limiting soil deformation. Li *et al.* (2013) studied the basal heave of a semi-covered excavation from the aspect of width-depth ratio and retaining structure size. Liu *et al.* (2019) proposed that the semi-covered supporting system is an asymmetric structure because of the cover plate and cover plate load, and discussed the deformation of the supporting structures. However, these researches mainly focused on a certain semi-covered excavation. The characteristics of semi-covered supporting structures are not discussed too much. In addition, the influence of building loads on the asymmetric supporting system is not mentioned. Tan *et al.* (2017) discussed the influence of a semi-covered deep excavation in Shanghai on the adjacent buildings through monitoring analysis and numerical simulation. The difference of deformation characteristics of excavations and retaining structures between semi-covered method, bottom-up method and top-down method was analyzed. However, it didn't show how adjacent buildings affect the semi-covered excavations, and the influence mechanism of the semi-covered structures was not revealed clearly enough. In addition, there is no research on the situation that the supporting structures doesn't embedded into rock under the condition of semi-covered excavation, and its rationality and reliability are worth discussing.

Based on the semi-covered deep excavation of Shanxi Road Subway Station in Nanjing, the shallow foundation building D and the pile foundation high-rise building C were selected as the existing buildings to discuss the establishment of the numerical model and the determination of the vehicle load on the cover plate. After verification by field data, the building storeys, the basement storeys, the pile length, the existence of the cover plate and the depth of the diaphragm walls were selected as variables, and 44 groups of simulation were designed. Based on the existing research results of the deep excavation deformation, the deformation response mechanism of semi-covered deep excavations under existing buildings was studied, and the coordination deformation mechanism between semi-covered supporting structures and excavations was discussed, so as to fill the gap in this field.

2. Engineering background

2.1 Project description

The Shanxi Road Subway Station is located in a busy city with heavy traffic in Nanjing, Jiangsu Province, China. The station is an underground two-storey island platform

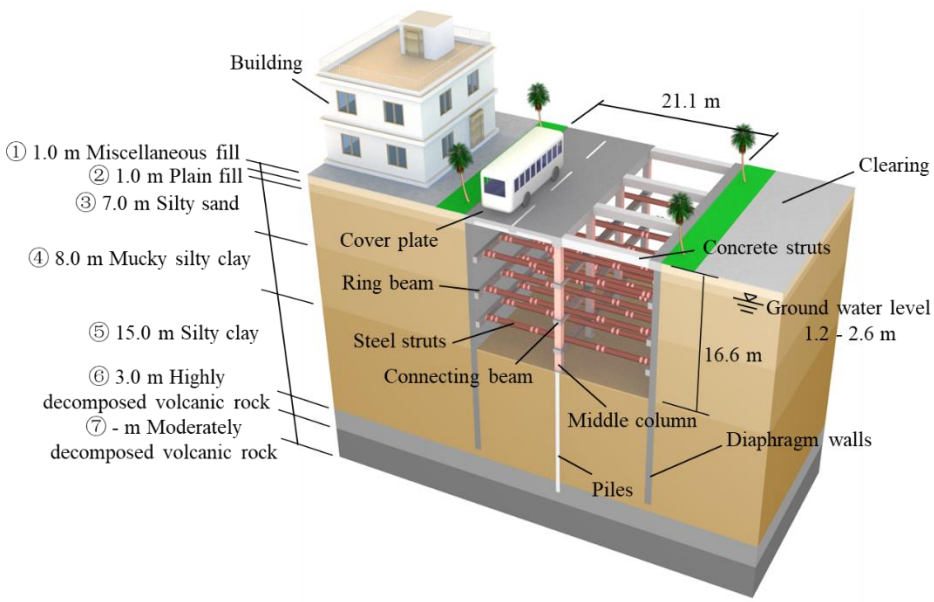

Fig. 2 Schematic diagram of the semi-covered deep excavation of Shanxi Road Subway Station

Table 1 Physical and mechanical parameters of the strata

Layer	Strata	Average thickness	Unit weight	M	λ	κ	v_λ	E	μ	c'	φ'	T
		m	kN/m^3	-	-	-	-	MPa	-	kPa	°	MPa
①	Miscellaneous fill	1.0	22.0	-	-	-	-	2	0.15	5.0	25.0	0.0
②	Plain fill	1.0	18.5	-	-	-	-	4	0.18	10.0	10.0	0.0
③	Silty sand	7.0	19.6	-	-	-	-	15	0.31	6.2	32.1	0.0
④	Mucky silty clay	8.0	17.6	0.98	0.128	0.024	3.3	6	0.39	14.4	17.0	0.0
⑤	Silty clay	15.0	19.5	1.13	0.088	0.017	3.3	12	0.30	35.5	15.6	0.0
⑥	Highly decomposed volcanic rock	3.0	22.0	-	-	-	-	130	0.23	100.0	33.0	7.0
⑦	Moderately decomposed volcanic rock	-	25.7	-	-	-	-	15000	0.19	300.0	36.0	10.0

(M is slope of the critical state line in q'-p' space for MCC; λ and κ are slopes of the normal consolidation curve and the rebound curve, respectively; v_λ is parameter determined by the position of the normal consolidation curve; E is Young's modulus; μ is Poisson's ratio; c' is effective cohesion; φ' is effective friction angle; T is tensile strength.)

station located at the intersection of North Zhongshan Road, West Shanxi Road and Hunan Road. The station is 272.80 m long and the width of the standard section and the end well are 21.10 m and 25.30 m, respectively. The depth of the standard section and the end well are 16.60 m and 17.93 m, respectively, with about 3.08 m depth soil above the roof. The location of the excavation and surrounding buildings are shown in Fig. 1. Limited by the site conditions, the semi-covered method is adopted, and the cover plate is used to relieve traffic. Fig. 2 shows the schematic diagram of the semi-covered supporting system of the excavation.

2.2 Ground condition

The foundation pit is located in the floodplain area of the Qinhuai River, where soft soil and sandy soil are thick.

The stratigraphic profile of the excavation can be seen in Fig. 2. The physical and mechanical parameters of the strata are shown in Table 1, in which part of the parameters were derived from the geological prospecting report made for the project, and parameters about MCC model were obtained from the laboratory test, including consolidated undrained triaxial shear test and isotropic consolidation test. The elastic modulus was determined as 3~5 times the compression modulus, the slope of the critical state line was determined according to consolidated undrained triaxial shear test, and the slopes of the normal consolidation curve and the rebound curve were determined according to isotropic consolidation test.

The excavation is located in a saturated weak pervious layer, with the ground water level of 1.20 m ~ 2.60 m, and an annual variation of about 1.0 m. The permeable layer is mainly consist of filled soil, silty sand and gravel layer, while the rest of the strata are relatively impermeable layer.

2.3 Surrounding buildings

The main buildings around the station are shown in Table 2, and the positional relations are shown in Fig. 3. The main characteristics of the surroundings are: 1) several buildings with different storeys and foundation forms are near the pit in

Table 2 The main buildings around the pit

Building	Location	Building storeys /Basement storeys	Structural form
A (Shanxi Road Department Store)	7.1 m south of the foundation pit	6/0	Frame structure, pile foundation with precast square piles (side length of 450 mm and pile length of 36 m)
B (Suning Universal)	25.6 m south of the foundation pit	8/3	Frame shear wall structure, basement burial depth of 13 m, pile foundation with bored piles (pile diameters of 800 mm and 1200 mm and pile length of 25 m)
C (Jinshan Mansion)	15.4 m south of the foundation pit	35/3	Frame structure, basement burial depth of 14 m, pile foundation with bored piles (pile diameters of 1000 mm and 1200 mm and pile length of 30 m)
D (Private house)	10.8 m south of the foundation pit	4/0	Brick and concrete structure, shallow foundation
E (Xinyong Culture and Sporting Goods Mall)	7.8 m south of the foundation pit	7/0	Brick and concrete structure, shallow foundation
F (Heping Studio Entertainment City)	6.5 m north of the foundation pit	5/1	Frame structure, pile foundation with precast square piles (side length of 450 mm and pile lengths of 23 m and 25 m)
G (Bank of Communications, Nanjing Sub-branch)	6.7 m north of the foundation pit	24/1	Frame structure, basement burial depth of 5.5 m, pile foundation with bored piles (pile diameter of 1200 mm and pile length of 33.8 m)

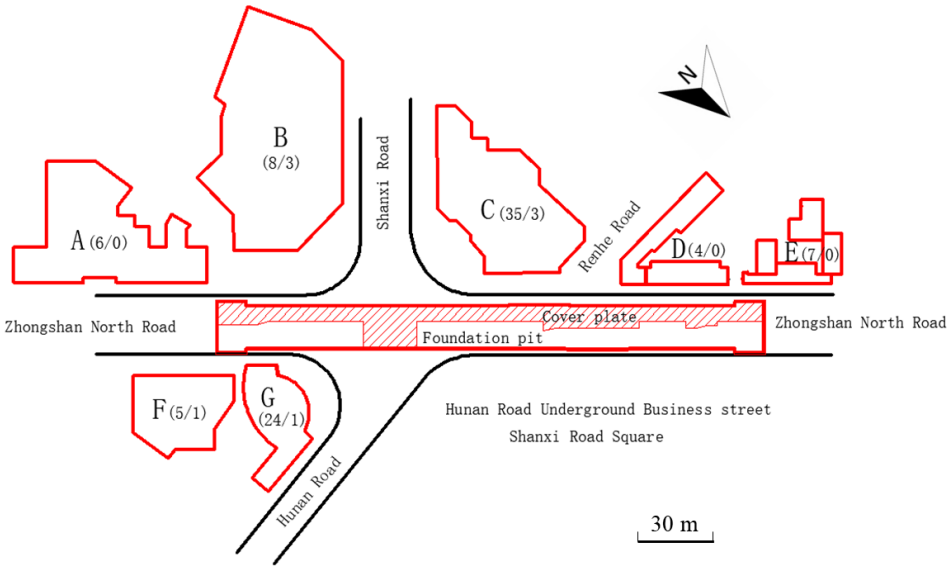

Fig. 3 Positional relations of the buildings around the station (A (6/0) means building A has 6 storeys and 0 basement storeys)

close distances; 2) one side of the pit is buildings while another side is clear. The asymmetric load on both sides will make the pit move to one side, thus enlarging the soil deformation around the buildings. Besides, different building storeys and foundation forms will reflect different responses to deformation. Many cases show that the buildings near the excavation often have large total settlement or heterogeneous settlement, and even cause the building cracking.

2.4 Construction procedure

It is divided into 12 construction sections along the length of the foundation pit, and each stage of construction is similar. The construction procedure of the standard section is shown in Fig. 4. In the process of the foundation pit excavation, tube well dewatering was used with open ditch drainage.

Each step in Fig. 4 is as follows:

①Constructing underground diaphragm walls, center columns and column piles;

②Excavating the first layers and constructing the first concrete struts and cover plate;

③Excavating the following layers and constructing the following steel struts;

④Constructing the concrete cushion and the main structure after excavating to the base;

⑤Removing the fourth struts and continue to constructing the main structure;

⑥Removing the second struts and finishing the construction of the main structure;

⑦Removing the remaining struts, cover plate and middle column, backfilling the soil.

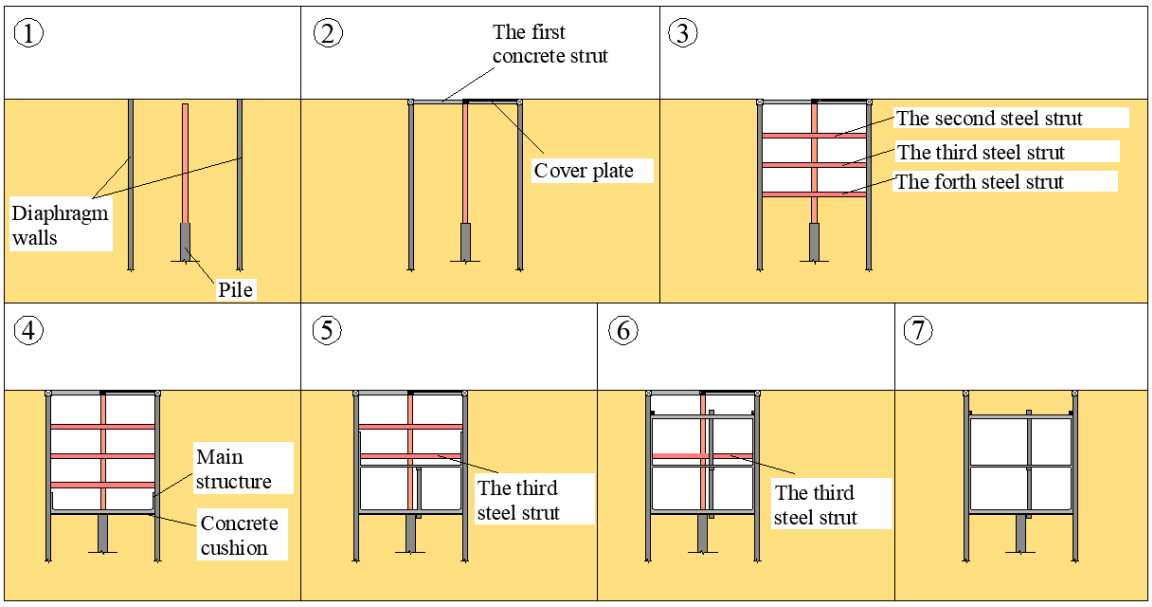

Fig. 4 Construction procedure of the standard section of the station

Table 3 Sizes and parameters of supporting structures

Supporting structure	Materials	Size mm	Density ρ kg/m^3	Elastic modulus E GPa	Poisson's ratio μ -
Underground diaphragm walls	C35 concrete HRB400 steel	800	2500	30	0.2
Concrete cover plate		300			
Concrete strut		800×1000			
Concrete pillar pile		φ1000			
Steel strut	Q345B steel	φ609×16	7800	200	0.3
Steel lattice column		500×500			

Underground diaphragm walls and four horizontal struts were used to supporting the excavation (as shown in Fig. 2). The penetration depths of the 800 mm thick underground diaphragm walls in the standard section and the end well are 13.50 m and 14.50 m, respectively, and the bottom of the diaphragm walls is in silty clay. The first strut is concrete strut with the horizontal spacing of 6.0 m, and half of which is covered with the 10.0 m wide cover plate. The other three are steel struts, with the horizontal spacing of 3.0 m and the vertical spacing of about 4.5 m. Specific sizes and parameters of supporting structures are shown in Table 3, in which the materials and size are from the design document, and other parameters were determined by referring to Yang's (2020) paper and Yu's (2018) paper.

3. Numerical simulation

3.1 Parameters

Numerical analyses were carried out using the 3D finite difference software FLAC^{3D}5.0, and Midas GTS NX was used to help building the model. The Modified Cam-Clay (MCC) model, which is based on the critical state theory, is one of the most widely used constitutive models for clay, and thus was used in the simulation of mucky silty clay and silty clay in the paper (Huang *et al.* 2011, Liu *et al.* 2019, Yang *et al.* 2020). And the remaining soils and rocks are calculated by Mohr-Coulomb model (Liu *et al.* 2019, Liu *et al.* 2022b). The physical and mechanical parameters of each layer are shown in Table 1.

In which, the friction constant M is the slope of the critical state line and can be calculated by the following formula

$$M = \frac{6\sin\varphi'}{3-\sin\varphi'} \tag{1}$$

Where φ' is the effective angle of internal friction.

λ and κ are the slopes of the normal consolidation curve and the rebound curve, respectively, and κ can be determined between (1/5 ~ 1/3) λ.

v_λ and p_1 are determined by the position of the normal consolidation curve. p_1 is generally assumed to be 1 kPa, then v_λ can be obtained by undrained shear strength c_u, friction constant M, λ and κ by the following formula

$$c_u = \frac{Mp_1}{2}\exp\left(\frac{\Gamma - v_{cr}}{\lambda}\right) \tag{2}$$

$$\Gamma = v_{\lambda} - (\lambda - \kappa)\ln(2) \tag{3}$$

Where Γ is the intercept of the normal consolidation curve on v axis, v_{cr} is the particular specific volume.

Bulk modulus K and shear modulus G can be calculated by

$$K = \frac{E}{3(1\text{-}2\mu)} \tag{4}$$

$$G = \frac{E}{2(1+\mu)} \tag{5}$$

Elastic constitutive model was adopted to reflect the constitutive relationships of the supporting structures, and the parameters were listed in Table 3. The parameters of the high-rise building basement are the same as that of diaphragm walls. The dimensions and parameters of pile foundation are the same as those of concrete column piles.

The parameters of the contact surface recommended in FLAC^{3D} manual is that the normal stiffness K_n and tangential stiffness K_s can be 10 times the equivalent stiffness of the surrounding "hardest" adjacent area (Yu *et al.* 2018), i.e.

$$K_n = K_s = 10 \max \left[\frac{\left(K + \frac{4}{3}G\right)}{\Delta z_{\min}} \right] \tag{6}$$

Where K is the bulk modulus of the surrounding "hardest" adjacent area, G is the shear modulus of the surrounding "hardest" adjacent area, and $\Delta z_{\min}$ is the minimum size of the connection area.

The cohesion c and friction angle φ of the contact surface can be 0.5 ~ 0.8 times of the adjacent soil layer.

The parameters of the contact surface are shown in Table 4, in which the parameters were determined through FLAC^{3D} manual and several trials until the contact surface shows correct contact behavior.

3.2 Cover plate load

3.2.1 Simplified method

The pavement slab is simplified as a plate model. Uniformly distributed load and concentrated load are both commonly used as load patterns.

(1) Uniformly distributed load

For the situation that vehicle is small and traffic flow is dense, it is more appropriate to make the vehicle load as uniformly distributed load. The uniformly distributed load is usually 10.0-20.0 kPa, and the value can reach 30.0 kPa when there is heavy construction equipment or heavy traffic (Shu 2019). The width is according to the actual situation, as Fig. 5(a) shows.

Table 4 Parameters of the contact surface

Location	Normal stiffness	Shear stiffness	Cohesion	Friction angle
	K_n GPa/m	K_s GPa/m	c kPa	φ °
Side of the wall	0.016	0.016	10	16
Bottom of the wall	0.15	0.15	70	23

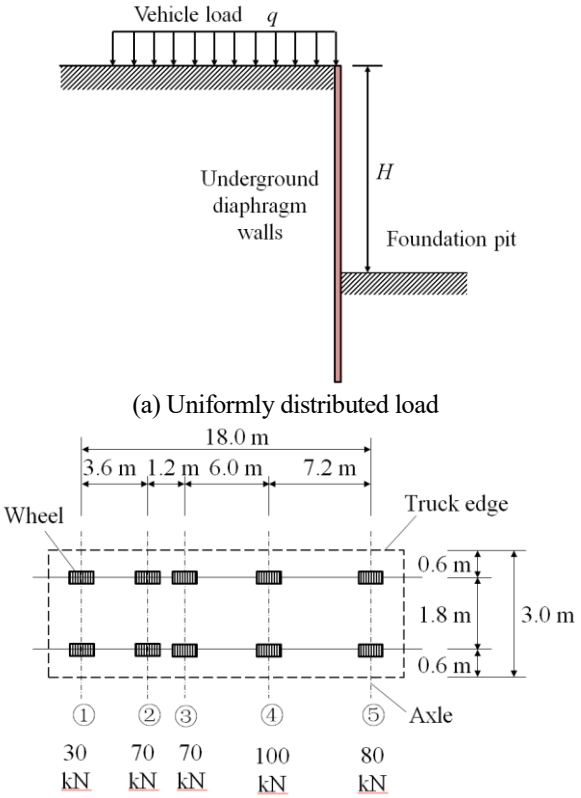

(a) Uniformly distributed load

(b) Concentrated load

Fig. 5 Simplified methods of vehicle loads

(2) Concentrated load

Generally, the load of heavy vehicles is considered to concentrated load, and the acting position is the center of the wheel (Shu 2019). According to the design document, the load of the temporary pavement system adopts the City-A class vehicle load standard in China, which stipulates the form that the five-axle truck is loaded with a total weight of 700.0 kN. The detailed load distribution is shown in Fig. 5(b).

The vehicle's dead weight load should be multiplied by the impact factor to reflect the impact of vehicle driving on the road surface according to *AASHTO LRFD Bridge Design Specifications (US-2007).The Standard of Loading for the Municipal Bridge Design (CJJ 77-1998)* in China stipulated that steel supports, rubber supports or reinforced concrete column piers and abutments, as well as the superstructures of steel bridge, reinforced concrete bridge, prestressed concrete bridge, concrete bridge and masonry arch bridge, should be designed considering the impact of vehicle loads. Multiply the car load by the impact factor μ to get the impact force of the car load, as is shown in the equation below

$$\mu = 0.6686 - 0.30321 \log L \tag{7}$$

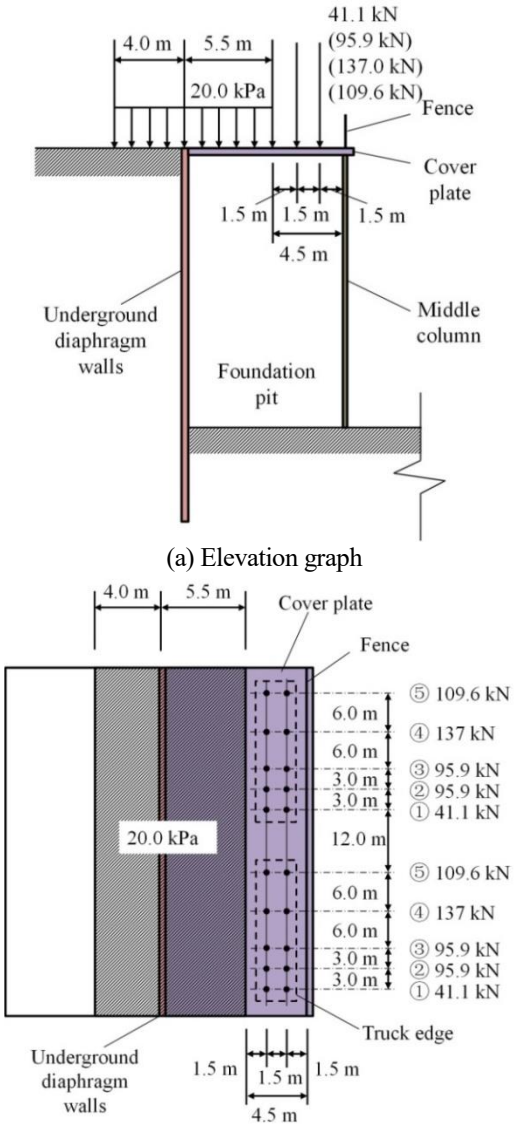

(a) Elevation graph

(b) Plan graph

Fig. 6 Load distribution on the cover plate in calculation model

Where L is the span of the superstructure (m).

The maximum impact factor μ shall not exceed 0.4

3.2.2 Cover plate load in simulation

According to the actual situation, the dregs truck running in the range of 4.5 m outside the diaphragm walls, the load of which was applied on the cover plate as the form of concentrated load. For security reasons, the distance between two dregs trucks should not be less than 8 m in actual construction, so the distance between the last wheel of the front truck and the first wheel of the rear truck was determined to be 12.0 m. A uniformly distributed load of 20.0 kPa was applied to 5.5 m inside the diaphragm walls and 4.0 m outside the diaphragm walls as normal traffic load (Shu 2019).

The span of the cover plate is 10.0 m, and the calculated impact factor μ is about 0.37. Considering the actual mesh size and the truck size, the load distribution of the cover plate in simulation is summarized in Fig. 6.

3.3 Calculating model

There are 7 buildings around the deep foundation pit. Considering the position and characteristics of the buildings, building D and building C were selected as examples to establish the numerical models and verify the accuracy of the simulation.

To eliminate the boundary effect, the left side of the model is 50.0 m from the pit edge, and the right side is 100.0 m and 144.0 m from the pit edge for building D and building C, respectively. The widths of the both models are 154.0 m. The heights of the models are 50.0 m because moderately decomposed volcanic rock is 18.0 m below the basal, which can resist deformation strongly. Building D is located 10.8 m from the edge of the excavation, with the range of 20.0 m, while building C is located 15.8 m from the edge of the excavation, with the range of 40.0 m. The simulation model of the building D contains 60824 nodes and 91820 elements, and those of the building C contains 270392 nodes and 301362 elements. The details of the models are shown in Fig. 7.

The bottom boundary of the models was fixed totally while the top surface was left free. The lateral sides of the model were fixed in the horizontal direction while vertical movement was allowed. The cover plate load was applied to the whole cover plate and in the range of 4.0 m outside the diaphragm walls. The building load was decided to be 15.0 kPa/floor. A concentrated force outside the foundation pit was applied at the joint of the steel struts and the diaphragm walls to simulate the pre-loading axial force of the steel struts, with the magnitude 800.0 kN for the first steel struts and 600.0 kN for the second and third steel struts according to the design document of the excavation. The initial groundwater level was set at 2.0 m under the surface, and was dewatered to 1.0 m below the excavation surface before each excavation step.

The detailed numerical simulation steps are: 1) initialing in-situ stress equilibrium; 2) defining the surrounding buildings and solving, setting the displacement to zero; 3) installing diaphragm walls, the first struts and the cover plate, excavating the first layer; 4) installing each struts and excavating each layer until to the bottom.

4 Comparison with field monitoring data

The deformation of excavations and retaining structures is usually concerned in engineering. Because of the few measuring points of surface settlement, there is no comparison about it.

4.1 Building D

Fig. 8 shows the deformation of the diaphragm walls and the building settlement of the building D section after excavation. Fig. 8(a) shows the lateral movement of the diaphragm walls, indicating that the monitoring data and the simulation results reflect the same characteristics. Affected by building and cover plate, the top of the diaphragm walls on both sides have the trends to moves away from the building. Besides, the asymmetric loads also lead to larger lateral movement of the building side. The maximum lateral

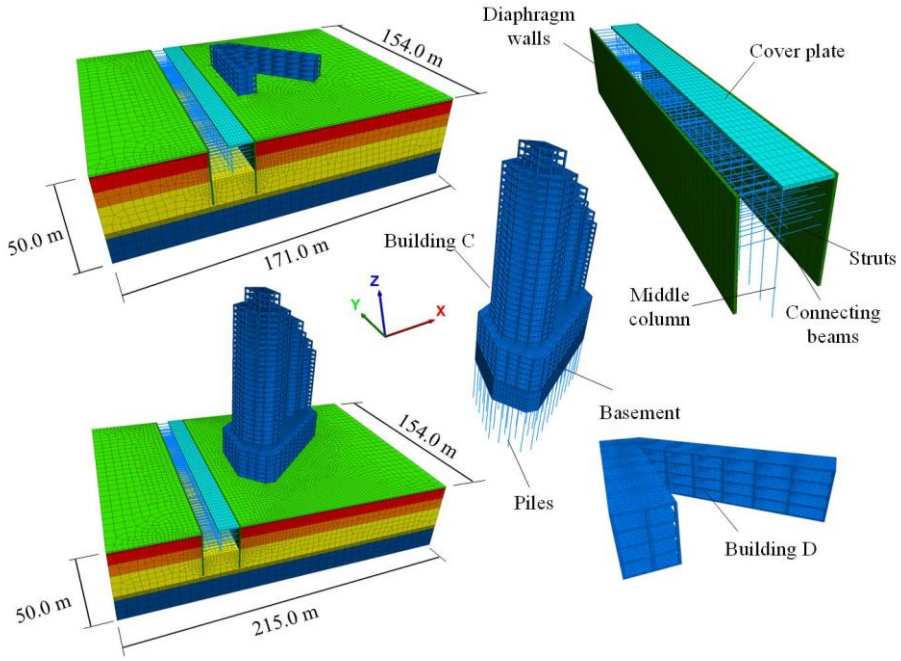

Fig. 7 Calculating models

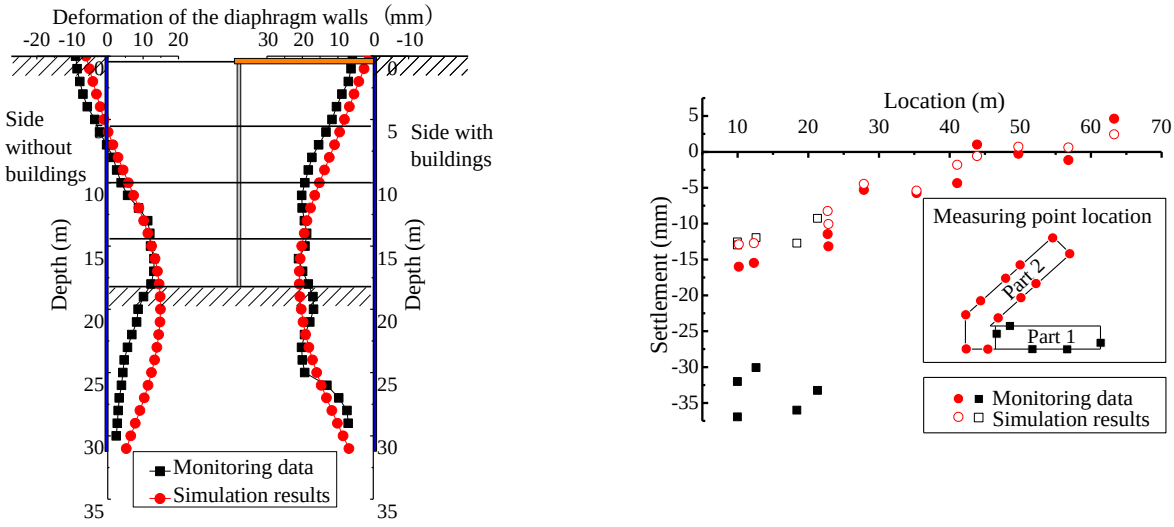

(a) Lateral movement of diaphragm walls (b) Building settlement

Fig. 8 Deformation of building D section after excavation (In Fig. 8 (a), positive value indicates movement into the pit)

displacement occurs on the excavation surface. Because the diaphragm walls are not embedded into rock, a certain lateral displacement into the pit was occurred on the bottom. Due to some actual interference factors, the monitoring data are more fluctuated along the depth, while the simulation results are relatively smooth.

Fig. 8 (b) shows the settlement of the building D. Due to the "L" shape of the building, it was constructed in two parts. There are sixteen settlement measuring points around the building D, of which five are located in part 1, and the remaining eleven are located in part 2 (Fig. 8(b)). It can be seen that the settlement of part 1 is larger than simulation, and the settlement of part 2 is in good agreement with simulation. The reason is that in simulation, the segmented construction of the building was ignored, resulting in the overall coordinated deformation of the two parts and the inconsistency between the simulation results and the monitoring results about part 1. In general, the building settlement is greater when the distance from the excavation is closer, and the relationship between the settlement value and the distance is obviously linear. The part away from the excavation even uplift due to the overall rotation of the building.

4.2 Building C

Fig. 9 shows the deformation of the diaphragm walls and the building settlement of the building C section after

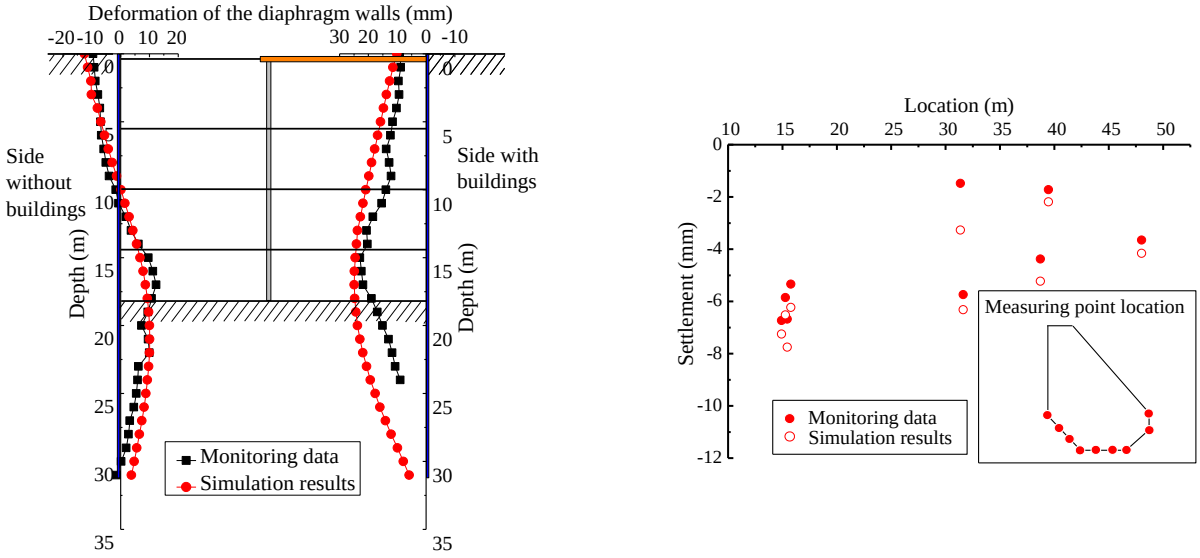

(a) Lateral movement of diaphragm walls (b) Building settlement

Fig. 9 Deformation of building C section after excavation (In Fig. 9 (a), positive value indicates movement into the pit)

excavation. Fig. 9(a) shows the lateral movement of the diaphragm walls. Similarly, due to the influence of building and cover plate, the top of the diaphragm walls tends to move to the non-building side, but the deviant value is bigger than that of the building D section (Fig. 8). Because of the big size and loads of the building C, the difference between the two diaphragm walls are more obvious. That is, the maximum lateral movement of the building side is larger than those of the non-building side and the position of the maximum lateral movement is higher than those of the non-building side.

Fig. 9(b) shows the influence of excavation on the settlement of building C. All nine settlement measuring points of the building C are near the excavation (Fig. 9(b)). In general, the numerical simulation is in good agreement with the monitoring, though simulation results are a little bigger than monitoring data. Compared with building D, the settlement of building C is smaller owing to the basement and pile foundation (compared with Fig. 8(b)). Besides, the settlement values present more obvious spatial effect because of the huge size and complicated structure.

5. Influencing factor analysis of deformation

5.1 Simulation conditions

The calculation results correspond well with the field data, and the parameters and boundary conditions are set reasonably, which can be used for further analysis. This section studies the influence of existing buildings by changing the height and the corresponding foundation form of the buildings, and the influence of supporting form by changing existence of the cover plate and depth of the diaphragm walls. The simulation groups are shown in Table 5. Notably, the bottom of the excavation is about 17.0 m, and the bottom of the diaphragm walls is about 31.0 m. By comparing groups 17 ~ 20 and groups 21 ~ 24 in Table 5, the influence of the relationship between the pile depth and the excavation depth on deformation can be obtained. By comparing groups 25 ~ 26 and groups 29 ~ 30 in Table 5, the influence of the relationship between the pile depth and the diaphragm walls depth on deformation can be obtained.

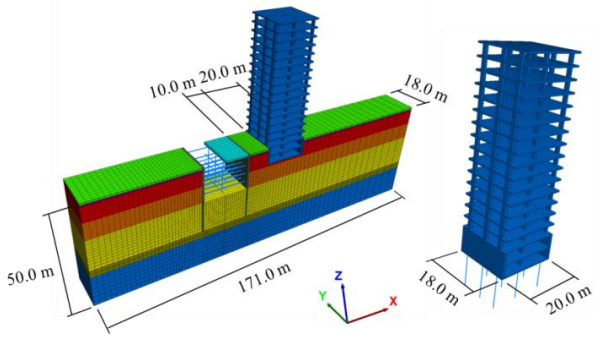

Fig. 10 Calculating model of group 21 as an example

To get general rules, some assumptions should be made in this section: 1) the building shape is a regular cuboid with a big size so that a plane strain model can be established into analysis; 2) the building range and location remains unchanged and is located at 10.0 m from the edge of the pit at the cover plate side (or the same position of the non-cover-plate groups), and the range is 20.0 m; 3) for high-rise buildings, the basement height is 4.0 m/floor and the pile cross section is the same as those of the building C. Other conditions including strata parameters, excavation sizes, boundary conditions, construction procedures and cover plate loads remain the same. Fig. 10 is the numerical calculating model of group 21 as an example with necessary sizes.

5.2 Lateral displacement of the diaphragm walls

Fig. 11 shows the maximum lateral displacement δ_{hm} and the depth of the maximum lateral displacement H_m of the diaphragm walls under 44 groups of calculation condition. For

Table 5 Simulation groups

Group	Surrounding buildings			Retaining structures	
	Building storeys	Basement storeys	Pile length/m	Existence of the cover plate	Depth of the diaphragm walls/m
1	0	0	0	Yes	31.0
2					35.0
3				No	31.0
4					35.0
5-8	4	0	0	Ditto	
9-12	8	0	0	Ditto	
13-16		1	0	Ditto	
17-20	15	1	11.0	Ditto	
21-24		2	11.0	Ditto	
25-28	25	2	21.0	Ditto	
29-32		3	21.0	Ditto	
33-36	35	3	30.0	Ditto	
37-40		4	30.0	Ditto	
41-44	50	4	30.0	Ditto	

Note: The building load is 15.0 kPa/floor and the basement height is 4.0 m/floor

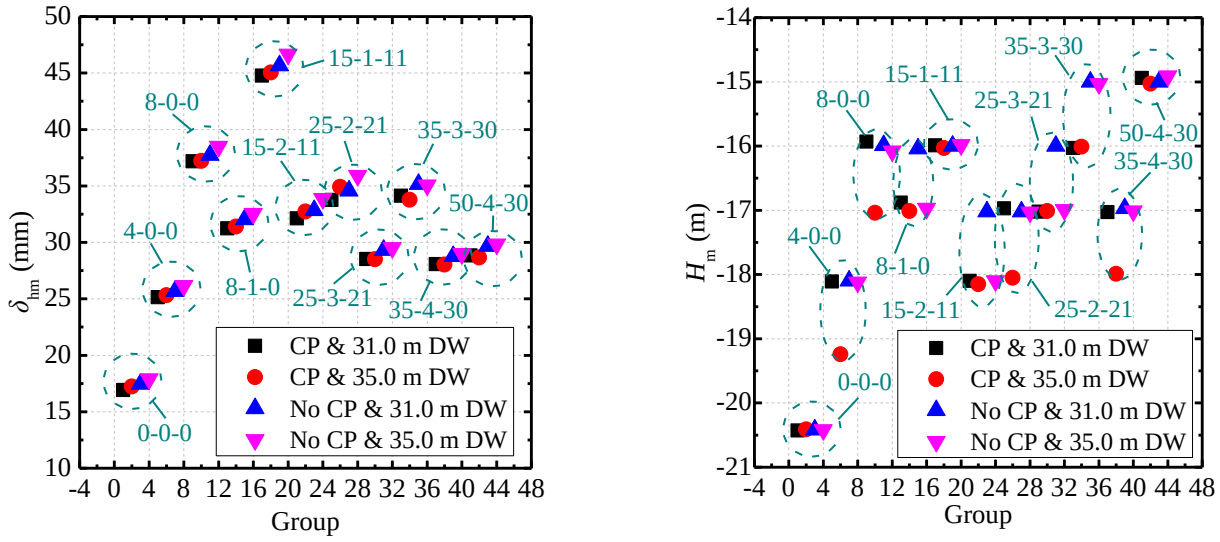

(a) Maximum lateral displacement δ_{hm} (b) Position of the maximum lateral displacement H_m

Fig. 11 The maximum lateral displacement of the diaphragm walls δ_{hm} and the corresponding position H_m under 44 groups of calculation condition (CP means cover plate, DW means diaphragm walls; in a-b-c, a means building storeys, b means basement storeys, c means pile length)

the convenience of analysis, it was named in the form of a-b-c according to different building conditions, where a means building storeys, b means basement storeys, c means pile length. Fig. 11(a) shows that when buildings and foundation forms are the same, existence of the cover plate and the depth of the diaphragm walls have little effect on δ_{hm}. In the first 20 groups (0-0-0 to 15-1-11), δ_{hm} increases significantly with the increase of the building storeys, but δ_{hm} decreases suddenly from 8-0-0 to 8-1-0, indicating that the increase of the basement storeys will significantly reduce the lateral displacement of the diaphragm walls. The same phenomenon also exists from 15-1-11 to 15-2-11, from 25-2-21 to 25-3-21, and from 35-3-30 to 35-4-30. From group 21 (15-2-11), since the pile depth reaches 19.0 m, which is deeper than excavation (17.0 m), the increasing of building storeys affects weaker on δ_{hm}. Compared between 35-4-30 and 50-4-30, because the pile is embedded into rock, the building load is mainly supported by rock stratum, so increasing of building storeys has little effect on the lateral displacement of diaphragm walls. Fig. 11 (b) shows that with the increase of the building storeys, the position gradually moves up, but it tends to move downward when basement storeys increases. When the building form is the same, the influences of the cover plate and the depth of the diaphragm walls on H_m are not regular. But in general, H_m is larger under the condition of CP & 31.0 m DW, and is smaller under the condition of No CP & 35.0 m DW, but the difference

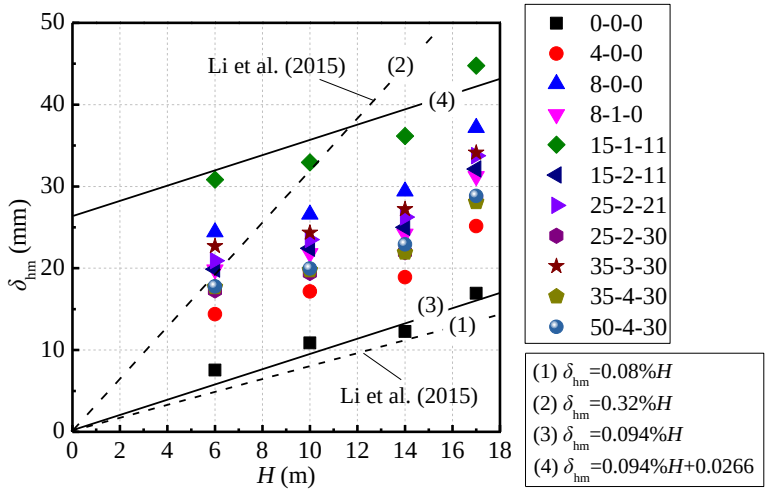

Fig. 12 Relationship between the maximum lateral displacement of the diaphragm walls δ_{hm} and excavation depth H (In a-b-c, a means building storeys, b means basement storeys, c means pile length)

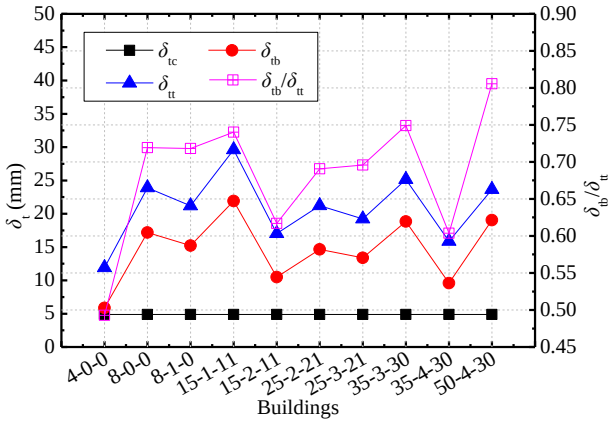

Fig. 13 Influence of buildings and cover plate on the top lateral displacement of the diaphragm walls (δ_{tc} means lateral movement of the top of the diaphragm walls caused by cover plate, δ_{tb} means lateral movement of the top of the diaphragm walls caused by buildings, δ_{tt} means lateral movement of the top of the diaphragm walls caused by both cover plate and buildings; In a-b-c, a means building storeys, b means basement storeys, c means pile length)

is within 1.0 m.

It can be seen that the main factor affecting δ_{hm} and H_m is the form of the existing buildings, instead of the cover plate and the depth of the diaphragm walls. Therefore, the conditionof CP & 31.0 m DW is selected to represent various building forms to discuss the relationship between the maximum lateral displacement of diaphragm walls and excavation depth H, as shown in Fig. 12. In Fig. 12, the dash lines (1) and (2) are the statistical data about the relationship between the maximum lateral displacement of the retaining structures of the subway station in Nanjing and the excavation depth obtained by Li *et al.* (2015), showing that the maximum lateral displacement of the retaining structures is between δ_{hm}=0.08%H and δ_{hm}=0.32%H. Comparison shows that most of the simulation results are within the range proposed by Li *et al.*, but to be more accurately, the maximum lateral displacement of the retaining structures is more appropriate between δ_{hm}=0.099%H and δ_{hm}=0.099%H+0.0245, and the correlation coefficient values R^2 are 0.987 and 0.832, respectively. Mainly because there is a large building load on the side of the excavation, which will lead to a large lateral displacement of the diaphragm walls in the early excavation

For semi-covered excavation, cover plate and existing buildings on one side will lead to asymmetric compression problem, and the effect degree of them on the lateral displacement of retaining structures is worth studying. Fig. 13 shows the top lateral displacement of diaphragm walls caused by buildings δ_{tb} and the cover plate δ_{tc} under different building conditions when the depth of the diaphragm walls is 31.0 m. The influence of the building on the diaphragm walls was obtained from the working condition without cover plate, the total influence of building and cover plate on the diaphragm walls was obtained from the working condition with cover plate, and the influence of the cover plate on the diaphragm walls was obtained from the difference between the two. In order to accurately reflect the levels of δ_{tb} and δ_{tc}, the lateral displacement in the figure is the difference between the lateral displacement of each group and that of group 3. As can be seen, δ_{tc} of each group is about 5.0 mm, while δ_{tb} is much larger, especially when building storeys is larger and basement storeys is fewer, for large building load will cause large top lateral displacement of the diaphragm walls. With the increase of building storeys, the law of δ_{tb} is very similar to that of the total top lateral displacement of the diaphragm walls (δ_{tt}), which shows that δ_{tb} and δ_{tt} increase with the increase of the building storeys and decreases with the increase of the basement storeys. The pink curve is the ratio of δ_{tb} to δ_{tt}, which reflects the contribution of the building load to the top lateral displacement of the diaphragm walls, and also reflects this rule.

Fig. 14(a) selects the building form 35-3-30 as an example, and shows the lateral displacement curve of the diaphragm walls of group 1, 3, 4, 34, 35 (the corresponding conditions are shown in Table 6). It can be seen that the cover plate mainly affects the deformation curve of the upper part of the

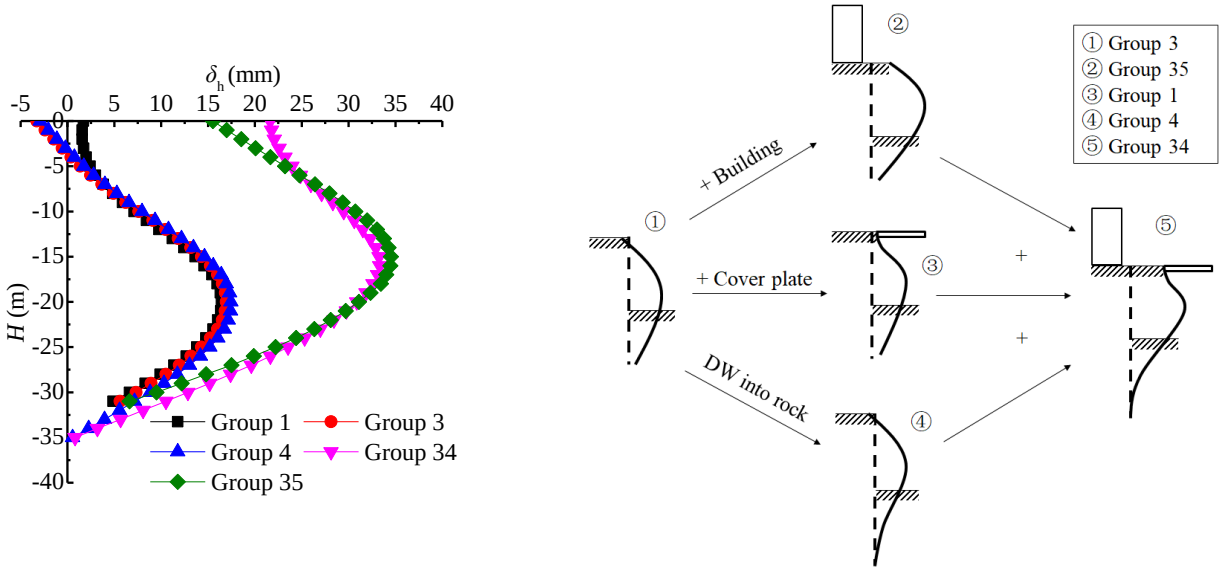

(a) Lateral displacement curve (b) Influence mechanism

Fig. 14 Influence of existing buildings, cover plate and the depth of the diaphragm walls on lateral displacement curve of the diaphragm walls (The corresponding operating conditions of group 1, 3, 4, 34, 35 are shown in Table 6)

diaphragm walls (groups 1, 34), owing to its relatively high stiffness. The diaphragm walls embedded into rock can greatly limit the bottom lateral displacement, but has little effect on the maximum lateral displacement (groups 4 and 34). So in practical engineering, it is safe to support with 31.0 m deep diaphragm walls. By subtracting the lateral displacement curves of diaphragm walls of group 35 and group 3, the influence of buildings on the lateral displacement of diaphragm walls can be reflected when the building form is 35-3-30.

Although the lateral displacement curves of diaphragm walls are different under different building loads and different foundation forms, and the maximum lateral displacement and corresponding location are also significantly different, the influence mechanism of existing buildings, cover plates and depth of diaphragm walls on the lateral displacement curve of diaphragm walls is the same. Fig. 14(b) summarizes the influence mechanism of these three factors from Fig. 14(a). It can be seen that the existing building causes the asymmetric pressure on one side to cause the lateral displacement curve of the diaphragm walls to move into the pit as a whole; The cover plate mainly affects the deformation of the upper part of the diaphragm walls, and the top of the diaphragm walls is warped by rigid connection between the cover plate and the diaphragm walls; The diaphragm walls embedded into rock limits the bottom lateral displacement and changes the shape of the lateral displacement curve at the bottom of the diaphragm walls. The conclusions can be extended to general situations.

5.3 Surface settlement

Fig. 15 shows the maximum surface settlement δ_{vm} outside the building side and the corresponding position d_m of 44 calculation conditions. When there is no basement and no piles, δ_{vm} increases significantly with the increase of the building storeys (0-0-0 to 8-0-0). When basement exists, due to the large stiffness of the basement, the ability to coordinate deformation is strong, greatly alleviate the surface settlement, which is consistent with other scholars' conclusion (Luat *et al.* 2020a, Luat *et al.* 2020b). In the following groups, due to the existence of the basement, δ_{vm} is always within 20 mm. High-rise buildings often use box foundation, on the one hand to meet the needs of underground parking, on the other hand, to alleviate the ground deformation and reduce the ground uneven settlement. Cover plate will slightly increase δ_{vm}, mainly because the cover plate load intensifies the asymmetric pressure of the excavation, making the diaphragm walls to move into the excavation, and finally leads to the deformation of the soil behind the wall. δ_{vm} is slightly larger when diaphragm walls embedded into rock (35.0 m). In the case of no buildings (0-0-0), d_m is about 12.0 m away from the edge of the pit without cover plate, and is slightly close to the pit with cover plate, which are all within the range of the maximum surface settlement position of soft soil excavations proposed by Clough and O'Rourke (1992). With the increase of the building storeys, d_m moves away from the pit, and is close to the outer boundary of the building when building storeys is 8 floors (8-0-0). Since the basement has a certain stiffness, when basement exists, the maximum settlement occurs at the edge of the basement near the excavation (about 10.0 m behind the wall), which is consistent with the conclusion of Tan *et al.* (2016). The cover plate and diaphragm walls will have an impact on d_m only when the floor building layer is low and there is no basement.

Similarly, the condition of CP & 31.0 m DW is selected to represent various building forms to discuss the relationship between the maximum surface settlement and excavation depth, as shown in Fig. 16. In Fig. 16, the dash lines (1) and (2) are the statistical data about the relationship between the maximum surface settlement outside the excavation of the subway station in Nanjing and the excavation depth obtained by Li *et al.* (2015), and it is found that δ_{vm} is between δ_{vm}=-0.04%H and δ_{vm}=-0.19%H. Although the simulation results are

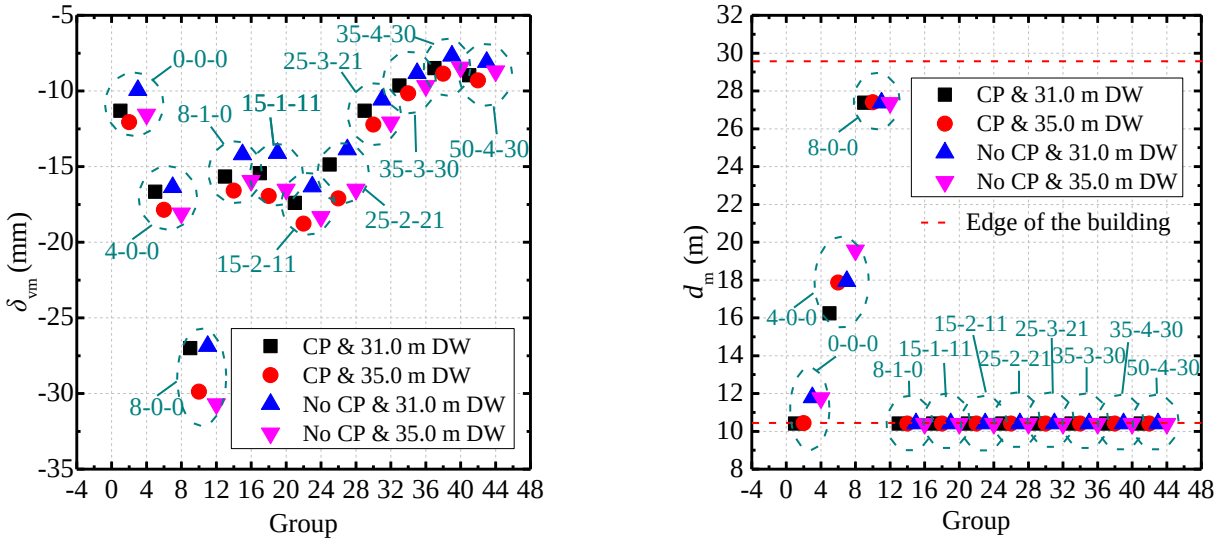

(a) Maximum surface settlement δ_{vm} (b) Position of the maximum surface settlement d_m

Fig. 15 The maximum surface settlement outside the pit δ_{vm} and the corresponding position d_m under 44 groups of calculation condition (CP means cover plate, DW means diaphragm walls; in a-b-c, a means building storeys, b means basement storeys, c means pile length)

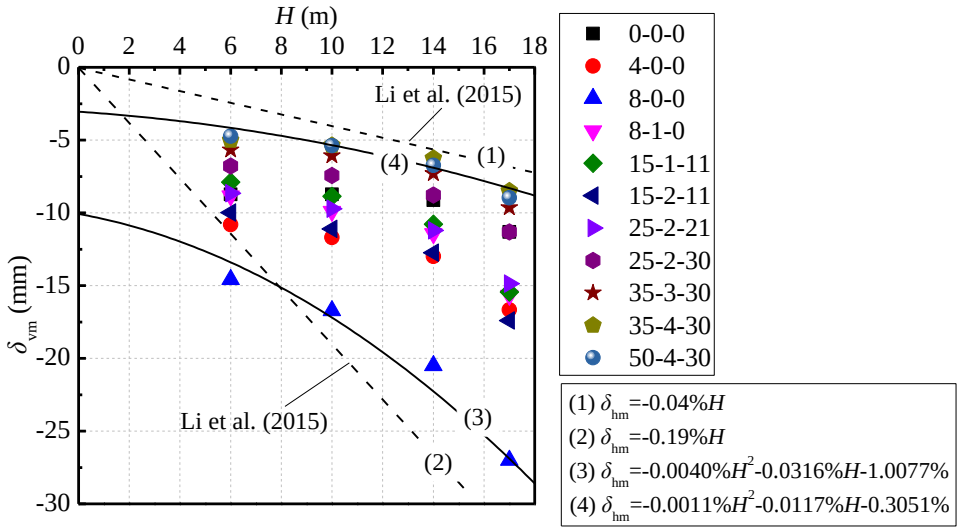

Fig. 16 The relationship between the maximum surface settlement δ_{vm} and excavation depth H (In a-b-c, a means building storeys, b means basement storeys, c means pile length)

in good agreement with the conclusions of Li *et al.*, it can still be seen that due to the existence of existing buildings, the distribution boundary of δ_{vm} presents a quadratic function trend. For the condition of existing buildings on one side, the relationship between the maximum surface settlement outside the pit and the excavation depth is between δ_{vm}=0.0040%H^2-0.0316%H-0.978% and δ_{vm}=0.0011%H^2-0.0117%H-0.320%, and the correlation coefficient values R^2 are 0.947 and 0.851, respectively.

Fig. 17 shows the soil settlement outside the pit under the condition of cover plate & 31.0 m diaphragm walls under different building forms. Because the pavement hardening is not considered in simulation, the settlement in a small range outside the diaphragm walls is larger. It can be seen that the excavation mainly affects the soil settlement in the triangle area within 30.0 m behind the wall, and the influence area haslittle relationship with the existing buildings and foundation forms. When there is a shallow foundation building outside the pit, the soil settlement outside the pit increases with the increase of building storeys, and the position of the maximum settlement tends to move outward. When basement exists, the maximum surface settlement occurs at the edge of the basement near the excavation (consistent with the conclusion in Fig. 15), and the building has a tendency of inward dumping. Basement can effectively reduce the soil settlement and control the settlement range due to the ability to coordinate deformation. When the pile foundation is longer enough, it can control the settlement of buildings and the surrounding soil through the friction with the surrounding soil and the bearing capacity of the pile end.

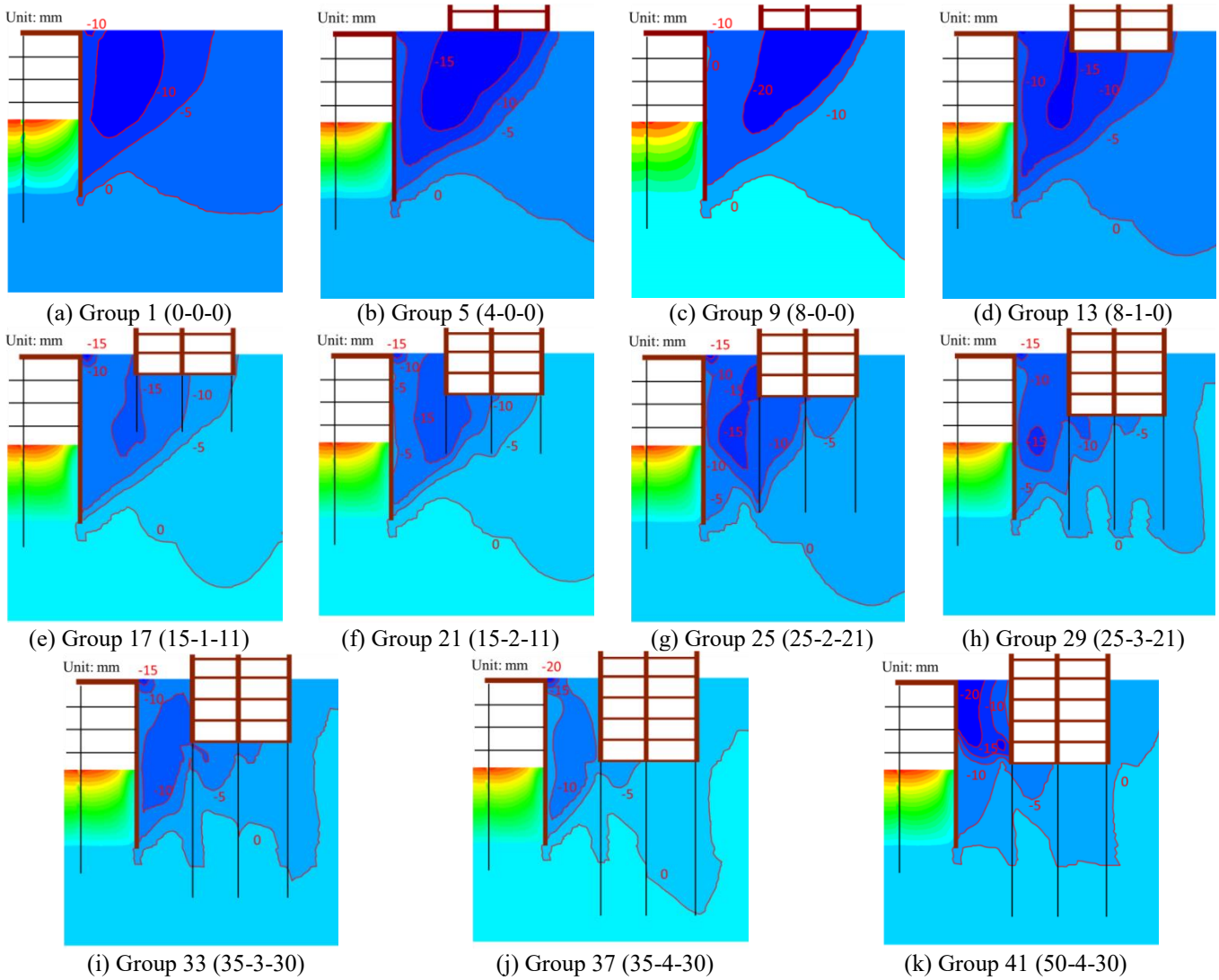

Fig. 17 The surface settlement outside the pit with cover plate & 31.0 m diaphragm walls under different existing buildings (Negative values indicate settlement and positive values indicate uplift. In a-b-c, a means building storeys, b means basement storeys, c means pile length)

6. Conclusions

Based on the semi-covered deep excavation of Shanxi Road Subway Station, the deformation response mechanism of semi-covered excavation under existing buildings was studied, and the coordinated deformation mechanism of semi-covered retaining structures and excavation was discussed. The following conclusions are drawn:

- δ_{hm} increases significantly with the increase of the building storeys, decreases significantly with the increase of the basement storeys, and is relatively stable when the pile depth is deeper. H_m gradually moves up with the increase of the building storeys, and downwards with the increase of the basement storeys. The maximum lateral displacement δ_{hm} is distributed between δ_{hm}=0.099%H and δ_{hm}=0.099%H+0.0245 due to large building load on one side.
- The lateral displacement of the top of the diaphragm walls caused by the cover plate is about 5.0 mm, while that caused by buildings is much larger, especially when building storeys is more and the basement storeys is less. The law of δ_{tb} is very similar to that of the total top lateral displacement δ_{tt}, showing that δ_{tb} and δ_{tt} increase with the increase of the building storeys and decreases with the increase of the basement storeys.
- The existing building causes the asymmetric pressure on one side to cause the lateral displacement curve of the diaphragm walls to move into the pit as a whole. The cover plate mainly affects the deformation of the upper part of the diaphragm walls, and the top of the diaphragm walls is warped by rigid connection between the cover plate and the diaphragm walls. The diaphragm walls embedded into rock limits the bottom lateral displacement and changes the shape of the lateral displacement curve at the bottom of the diaphragm walls, but has little effect on the maximum lateral displacement.
- The cover plate and the depth of the diaphragm walls

have little effect on the maximum surface settlement outside the pit δ_{vm}. δ_{vm} increases significantly with the increase of the shallow foundation building storeys. Because of the good coordinated deformation capacity of basement and pile foundation, δ_{vm} changes little with building layers and within 20 mm. With the increase of the building storeys, the position of the maximum ground settlement d_m moves away from the pit, and is close to the outside boundary of the building when building storeys is 8 floors (8-0-0). When basement exists, the maximum settlement occurs at the edge of the basement near the excavation (about 10.0 m behind the wall). Existing buildings make the relationship between the maximum surface settlement outside the pit and the excavation depth following between δ_{vm}=0.0040%H^2-0.0316%H-0.978% and δ_{vm}=0.0011%H^2-0.0117%H-0.320%.

- Excavation mainly affects the settlement of soil in triangle area within 30.0 m behind the wall, and the influence area has little relationship with the existing buildings and foundation forms. Longer pile foundation can control the settlement of buildings and the surrounding soil through the friction with the surrounding soil and the bearing capacity of the pile end.

Acknowledgements

The study is supported by National Natural Science Foundation of China (Grant No. 41972266), Chongqing Postdoctoral Natural Science Foundation of China (Grant No. cstc2019jcyj-bshX0072) and Graduate Scientific Research and Innovation Foundation of Chongqing, China (Grant No. CYB20031).

References

American Association of State Highway and Transportation Officials (2007), *The AASHTO LRFD Bridge Design Specifications (US-2007)*. American Association of State Highway and Transportation Officials, Washington, DC, USA.

Arboleda-Monsalve, L.G. and Finno, R.J. (2015), "Influence of concrete time-dependent effects on the performance of top-down construction", *J. Geotech. Geoenviron. Eng.*, **141**, 985-994. https://doi.org/10.1061/(ASCE)GT.1943-5606.0001260.

Capraru, C., amd Adam, D. (2014), "Evaluating the influence of deep excavations on neighbouring buildings by numerical analysis", *Proceedings of the 8th European conference on Numerical Methods in Geotechnical Engineering*, Delft, The Netherlands, Jun.

Chen, R.P., Li, Z.C., Chen, Y.M., Ou, C.Y., Hu, Q., and Rao, M. (2015), "Failure investigation at a collapsed deep excavation in very sensitive organic soft clay", *J. Perform. Constr. Fac.*, **29**(3), 04014078. https://doi.org/10.1061/(ASCE)CF.1943-5509.0000557.

Clough, G.W., and O'Rourke, T.D. (1992), "Closure to "Construction induced movements of in situ walls" by G. W. Clough and Thomas D. O'Rourke (June 18–21, 1990, No. 25)", *J. Geotech. Eng.*, **118**(4), 665-666. https://doi.org/10.1061/(ASCE)0733-9410(1992)118:4(665).

Guo, P.P., Gong, X.N. and Wang, Y.X. (2019), "Displacement and force analyses of braced structure of deep excavation considering unsymmetrical surcharge effect", *Comput. Geotech.*, **113**, 103102. https://doi.org/10.1016/j.compgeo.2019.103102.

Houhou, M.N., Emeriault, F. and Belounar, A. (2019), "Three-dimensional numerical back-analysis of a monitored deep excavation retained by strutted diaphragm walls", *Tunn. Undergr. Sp. Tech.*, **83**, 153-164. https://doi.org/10.1016/j.tust.2018.09.013.

Hsiung, B.C.B., Yang, K.H., Aila, W. and Ge, L. (2018), "Evaluation of the wall deflections of a deep excavation in Central Jakarta using three-dimensional modeling", *Tunn. Undergr. Sp. Tech.*, **72**, 84-96. https://doi.org/10.1016/j.tust.2017.11.013.

Hsiung, B.C.B., Yang, K.H., Aila, W. and Hung, C. (2016), "Three-dimensional effects of a deep excavation on wall deflections in loose to medium dense sands", *Comput. Geotech.*, **80**, 138-151. https://doi.org/10.1016/j.compgeo.2016.07.001.

Huang, M.S., Liu, Y.H. and Sheng, D.C. (2011), "Simulation of yielding and stress-stain behavior of Shanghai soft clay", *Comput. Geotech.*, **38**(3), 341-353. https://doi.org/10.1016/j.compgeo.2010.12.005.

Jamsawang, P., Jamnam, S., Jongpradist, P., Tanseng, P. and Horpibulsuk, S. (2017), "Numerical analysis of lateral movements and strut forces in deep cement mixing walls with top-down construction in soft clay", *Comput. Geotech.*, **88**, 174-181. https://doi.org/10.1016/j.compgeo.2017.03.018.

Jamsawang, P., Voottipruex, P., Tanseng, P., Jongpradist, P., and Bergado, D.T. (2019), "Effectiveness of deep cement mixing walls with top-down construction for deep excavations in soft clay: case study and 3D simulation", *ACTA Geotechnica*, **14**(1), 225-246. https://doi.org/10.1007/s11440-018-0660-7.

Khoiri, M., and Ou, C.Y. (2013), "Evaluation of deformation parameter for deep excavation in sand through case histories," *Comput. Geotech.*, **47**, 57-67. https://doi.org/10.1016/j.compgeo.2012.06.009.

Korff, M. (2013), "Response of piled buildings to the construction of deep excavations", Ph.D. Dissertation, Univ. of Cambridge, Cambridge, U.K.

Li, A.G., Li, Y.L. and Zhao, X.W. (2013), "Deformation research of temporary road and bridge system in semi top-down pit with gradual width", *Adv. Civil Eng.*, **256-259**, 1715-1720. https://doi.org/10.4028/www.scientific.net/AMM.256-259.1715.

Li, D.P., Li, Z.Q. and Tang, D.G. (2015), "Three-dimensional effects on deformation of deep excavations", *Geotech. Eng.*, **168**(6), 551-562. https://doi.org/10.1680/jgeen.15.00042.

Li, H.J., Liu, S.Y. and Tong, L.Y. (2019), "Evaluation of lateral response of single piles to adjacent excavation using data from cone penetration tests", *Can. Geotech. J.*, **56**(2), 236-248. https://doi.org/10.1139/cgj-2018-0131.

Likitlersuang, S., Surarak, C., Wanatowski, D., Oh, E. and Balasubramaniam, A. (2013), "Finite element analysis of a deep excavation: A case study from the Bangkok MRT", *Soils Found.*, **53**(5), 756-773. https://doi.org/10.1016/j.sandf.2013.08.013.

Lim, A., Hsieh, P.G. and Ou, C.Y. (2016), "Evaluation of buttress wall shapes to limit movements induced by deep excavation", *Comput. Geotech.*, **78**, 155-170. https://doi.org/10.1016/j.compgeo.2016.05.012.

Liu, S.H., Yang, J.S., Fu, J.Y. and Zheng, X.C. (2019), "Performance of a deep excavation irregular supporting structure subjected to asymmetric loading", *Int. J. Geomech.*, **19**(7), 05019007. https://doi.org/10.1061/(ASCE)GM.1943-5622.0001468.

Liu, X.R., Liu, P., Zhou, X.H., Wang, L.F., Zhong, Z.L., Lou X.H., Chen, T. and Zhang, J.L. (2022a), "Influence characteristics of isolation piles on deformation of existing shallow foundation buildings under deep excavation", *Geomech. Eng.*, **31**(1), 1-14. https://doi.org/10.12989/gae.2022.31.1.001.

Liu, X.R., Wang, L.F., Zhou, X.H., Wang, J.M., Zhong, Z.L., Liu, P., Xiong, F. and He, C.M. (2022b), "E-M calculation model and its application of calculating deformation in a new tunnel orthogonally undercrossing an existing tunnel", *Tunn. Undergr. Sp. Tech.*, **123**, 104418. https://doi.org/10.1016/j.tust.2022.104418.

Luat, N.V., Lee, K. and Thai, D.K. (2020b), "Application of artificial

neural networks in settlement prediction of shallow foundations on sandy soils", *Geomech. Eng.*, **20**(5), 385-397. https://doi.org/10.12989/gae.2020.20.5.385.

Luat, N.V., Nguyen, V.Q., Lee, S., Woo, S. and Lee, K. (2020a), "An evolutionary hybrid optimization of MARS model in predicting settlement of shallow foundations on sandy soils", *Geomech. Eng.*, **21**(6), 583-598. https://doi.org/10.12989/gae.2020.21.6.583.

Mansouri, H., and Asghari K.E. (2019), "Two dimensional finite element modeling of Tabriz metro underground station L2-S17 in the marly layers", *Geomech. Eng.*, **19**(4), 315-327. https://doi.org/10.12989/gae.2019.19.4.315.

Ministry of Construction, People's Republic of China (1998), *The Standard of Loading for the Municipal Bridge Design (CJJ 77-1998)*. China Building Industry Press, Beijing, China. (in Chinese)

Mitchell, A.R., Izumi, C., Bell, B.C. and Brunton, S. (2000), "Semi top-down construction method for Singapore MRT, NEL", *Proceedings of the International Conference on Tunnels and Underground Structures*, Singapore, Singapore, Nov.

Ng, C.W.W., Wei, J., Poulos, H. and Liu, H. (2017), "Effects of multipropped excavation on an adjacent floating pile", *J. Geotech. Geoenviron. Eng.*, **143**(7), 04017021. https://doi.org/10.1061/(ASCE)GT.1943-5606.0001696.

Nisha, J.J., Muttharam, M., Vinoth, M. and Prasad, C.R.E. (2019), "Design, construction and uncertainties of a deep excavation adjacent to the high-rise building", *Indian Geotech. J.*, **49**(5), 580-594. https://doi.org/10.1007/s40098-019-00368-4.

Orazalin, Z.Y., Whittle, A.J. and Olsen, M.B. (2015), "Three-dimensional analyses of excavation support system for the stata center basement on the MIT campus", *J. Geotech. Geoenviron. Eng.*, **141**(7), 05015001. https://doi.org/10.1061/(ASCE)GT.1943-5606.0001326.

Qian, J.G., Tong Y.M., Mu L.L., Lu Q. and Zhao H.Q. (2020), "A displacement controlled method for evaluating ground settlement induced by excavation in clay", *Geomech. Eng.*, **20**(4), 275-285. https://doi.org/10.12989/gae.2020.20.4.275.

Rotisciani, G.M., Miliziano, S. and Sacconi, S. (2016), "Design, construction, and monitoring of a building with deep basements in Rome", *Can. Geotech. J.*, **53**(2), 210-224. https://doi.org/10.1139/cgj-2015-0244.

Shu, X.L. (2019), "Study on stress and deformation characteristics ofsemi-rigid and semi-cover excavation system", M.sc. Dissertation, East China Jiaotong University, Nanchang, China (in Chinese)

Soomro, M.A., Mangnejo, D.A., Bhanbhro, R., Memon, N.A. and Memon, M.A. (2019), "3D finite element analysis of pile responses to adjacent excavation in soft clay: Effects of different excavation depths systems relative to a floating pile", *Tunn. Undergr. Sp. Tech.*, **86**, 138-155. https://doi.org/10.1016/j.tust.2019.01.012.

Talha, S.B. (2001), "Deformation behaviour of a retaining wall for a deep basement excavation with semi-top down method", *Proceedings of the 14th Southeast Asian Geotechnical Conference*, Hong Kong, China, Dec.

Tan, Y. and Wang, D.L. (2013), "Characteristics of a large-scale deep foundation pit excavated by the central-island technique in Shanghai soft clay. I: bottom-up construction of the central cylindrical shaft", *J. Geotech. Geoenviron. Eng.*, **139**(11), 1875-1893. https://doi.org/10.1061/(ASCE)GT.1943-5606.0000928.

Tan, Y., Zhu, H.H., Peng, F.L., Karlsrud, K. and Wei, B. (2017), "Characterization of semi-top-down excavation for subway station in Shanghai soft ground", *Tunn. Undergr. Sp. Tech.*, **68**, 244-261. https://doi.org/10.1016/j.tust.2017.05.028.

Tian, H., Tan, S.A., Tjahyono, S., Lim, C.H. and Tanaka, H. (2010), "Ground improvement for deep excavation of city square mall," *Proceedings of the 1st International Symposium on Ground Inprovement Technologies and Case Histories*, Singapore, Singapore, Dec.

Xiang, Y.Z., Goh, A.T.C., Zhang, W.G. and Zhang, R.H. (2018), "A multivariate adaptive regression splines model for estimation of maximum wall deflections induced by braced excavation," *Geomech. Eng.*, **14**(4), 315-324. https://doi.org/10.12989/gae.2018.14.4.315.

Yang, X.H., Jia, M.C. and Ye, J.Z. (2020), "Method for estimating wall deflection of narrow excavations in clay", *Comput. Geotech.*, 117, 103224. https://doi.org/10.1016/j.compgeo.2019.103224.

Yu, Y., Sun, H.Y. and Juang, C.H. (2018), "A new model for response of laterally loaded piles in soil-rock mixtures", *Comput. Geotech.*, **104**, 237-246. https://doi.org/10.1016/j.compgeo.2018.08.021.

Zhang, W.G., Zhang, R.H. and Goh, A.T.C. (2018), "MARS inverse analysis of soil and wall properties for braced excavations in clays," *Geomech. Eng.*, **16**(6), 577-588. https://doi.org/10.12989/gae.2018.16.6.577.

Zhang, R.H., Zhang, W.G. and Goh, A.T.C. (2018), "A simple model for ground surface settlement induced by braced excavation subjected to a significant groundwater drawdown" *Geomech. Eng.*, **16**(6), 635-642. https://doi.org/10.12989/gae.2018.16.6.635.

Zheng, G., Peng, S.Y., Ng, C.W.W., and Diao, Y. (2012), "Excavation effects on pile behaviour and capacity", *Can. Geotech. J.*, **49**(12), 1347-1356. https://doi.org/10.1139/t2012-095.

CC